

Exciton transport in the PE545 complex: insight from atomistic QM/MM-based quantum master equations and elastic network models

Sima Pouyandeh^{1,2,3}, Stefano Iubini^{3,4}, Sandro Jurinovich⁵,
Yasser Omar^{1,2}, Benedetta Mennucci⁵, Francesco Piazza^{3,6}

¹ Instituto de Telecomunicações, Physics of Information and Quantum Technologies Group, Portugal

² Instituto Superior Técnico, Universidade de Lisboa, Portugal

³ Centre de Biophysique Moléculaire, (CBM), CNRS UPR 4301, Rue C. Sadron, 45071, Orléans, France

⁴ Dipartimento di Fisica, Università di Firenze and INFN, Sezione di Firenze, Via G. Sansone 1, 50019 Sesto F.no (FI), Italy

⁵ Dipartimento di Chimica e Chimica Industriale, University of Pisa, via G. Moruzzi 13, 56124 Pisa, Italy

⁶ Université d'Orléans, Château de la Source, F-45071 Orléans Cedex, France

E-mail: Francesco.Piazza@cnrs-orleans.fr

Abstract. In this paper we work out a parameterization of the environment noise within the Haken-Strobl-Reinenker (HSR) model for the PE545 light-harvesting complex based on atomic-level quantum mechanics/molecular mechanics (QM/MM) simulations. We use this approach to investigate the role of different auto- and cross-correlations in the HSR noise tensor, confirming that site-energy autocorrelations (pure dephasing) terms dominate the noise-induced exciton mobility enhancement, followed by site energy-coupling cross-correlations for specific triplets of pigments. Interestingly, several cross-correlations of the latter kind, together with coupling-coupling cross-correlations, display clear low-frequency signatures in their spectral densities in the region 30-70 inverse centimeters. These slow components lie at the limits of validity of the HSR approach, requiring that environmental fluctuations be faster than typical exciton transfer time scales. We show that a simple coarse-grained elastic-network-model (ENM) analysis of the PE545 protein naturally spotlights collective normal modes in this frequency range, that represent specific concerted motions of the subnetwork of cysteines that are covalently linked to the pigments. This analysis strongly suggests that protein scaffolds in light-harvesting complexes are able to express specific collective, low-frequency normal modes providing a fold-rooted blueprint of exciton transport pathways. We speculate that ENM-based mixed quantum classical methods, such as Ehrenfest dynamics, might be promising tools to disentangle the fundamental designing principles of these dynamical processes in natural and artificial light-harvesting structures.

PACS numbers: 71.35.-y, 03.65.Yz, 87.15.-v, 87.15.H-

Keywords: quantum master equations, PE545 complex, bilins, elastic network models

Submitted to: *Phys. Biol.*

Contents

1	Introduction	2
2	Reduced quantum master equation from QM/MM simulations	4
2.1	Microscopic description of the exciton environment	6
3	HSR coefficients: the white noise approximation	7
3.1	Exciton transfer efficiency	11
4	HSR coefficients: an elastic-network analysis reveals specific low-frequency normal modes	14
5	Conclusions and perspectives	18

1. Introduction

Environmental effects can strongly influence the dynamics of quantum excitations in complex media. In the context of photosynthetic complexes [1, 2], a crucial role is played by the ultrafast process that allows to transfer the energy absorbed by the pigments from photons to the reaction center during the early stages of photosynthesis. In this respect, one of most relevant issues concerns the mechanisms that allow a fast and efficient energy transfer within the complex. The presence of a noisy protein scaffold that embeds the pigment network represents an essential feature of the problem. Indeed, at the microscopic level chromophores experience environment vibrations [3] that produce fluctuations of the local pigment site-energies and pigment-pigment couplings. Additionally, very slow protein motions contribute to add static disorder to the unperturbed exciton dynamics.

One of the key findings of recent theoretical research is that in certain regimes noise can act as a positive factor for transport efficiency. In particular, it has been shown [4, 5, 6] that exciton transfer efficiency can be enhanced by pure dephasing noise, that accounts for site-energy fluctuations due to protein vibrations. Optimal transport efficiency was found for intermediate amplitudes of the noise strength, in a region of the parameters compatible with room temperature conditions. The reason why a certain amount of dephasing is beneficial is that external fluctuations may promote excitonic transitions that speed up the global transfer process.

Understanding the role of environmental effects on the exciton dynamics necessarily requires a microscopic description of the environment-induced fluctuations on the electronic degrees of freedom. Extensive studies [3, 7, 8, 9, 10] have been performed in order to understand the role of spatio-temporal noise correlations in site-energy fluctuations and the presence of specific vibrational modes that interact with the electronic ones. Although in photosynthetic systems site-energy fluctuations are considerably larger than fluctuations in the site-site coupling energies [11, 12], it has been shown by Silbey and co-workers [13, 14] that even small, correlated coupling fluctuations may have a deep impact for speeding up the energy transfer process. Moreover, it was found that nonvanishing correlations between site-energy and coupling fluctuations may strongly enhance or suppress long-lived oscillations in populations, depending on the sign of the correlation. These effects were initially studied within a generalized Haken-Strobl-Reineker (HSR) model [15, 16], where

external environmental fluctuations are described in terms of classical Gaussian Markov processes (white noise). Further studies by Huo and Coker [17] performed with refined numerical techniques [18] along with more recent ones by other groups [19, 20, 21] using different modified quantum master equation (QME) approaches showed that the same phenomenology persists also with explicit non-Markovian harmonic models of heat bath.

In this paper we focus on the dynamics of the phycoerythrin 545 (PE545) light-harvesting complex of the marine cryptophyte alga *Rhodomonas* sp. strain CS24, that comprises 8 bilins [22, 23, 24, 25], see Fig. 1. This system absorbs very efficiently incident sunlight. Interestingly, recent studies ascribed this efficiency to the structural flexibility of the pigments, which allows the modulation of their absorption energy through local pigment-protein interactions [12]. This light-harvesting system seems to work as a *funnel*, that drives to the surface the excitons formed in the core of the complex, i.e. at the two strongly coupled PEB 50/61 pigments (see Fig. 1). This in turn is believed to facilitate the transfer of the excitonic energy to another complex in the neighborhood or to the reaction center, where the charge separation process may occur [12]. What is even more interesting, in a recent paper some of the present authors have shown that the spectral densities of individual pigments of PE545 may be very different with respect to those averaged over pseudo-symmetric pairs or over all pigments [26]. This strongly warns against an uniform parameterization of excessively simplistic quantum master equation approaches, such as Ref. [4], where a single dephasing rate is assumed to describe the whole extent of possible correlations. Rather, the need for a proper *ab-initio* parameterization of QME-based methods is apparent, as it is the whole range of possible correlations (site-energy/site-energy, coupling/coupling and site-energy/coupling) that appears to contain the fine details of phonon-mediated exciton transport in light-harvesting proteins.

The aim of this paper is to clarify the role and the relative weight of the different types of correlations among fluctuations, involving both site energies and coupling strengths, by parametrizing a general HSR quantum master equation directly from atomistic Quantum-Mechanics/Molecular-Mechanics (QM/MM) simulations. In section 2, we describe this procedure with the aim of computing the transport parameters of the complex at room temperature and study their dependence on the strength of the environment-induced perturbations. Accordingly, in section 3 we show that the so-called Zeno regime [4, 27], corresponding to a drop in exciton transfer efficiency at high noise strength is suppressed by coupling fluctuations at high temperature. However, while the Zeno regime might be relevant for some materials, as it has been already been shown by some of the present authors [28], it is certainly *de facto* inaccessible to biological macromolecules, as the protein scaffolds would fall apart well before reaching such high temperatures. From a theoretical standpoint, we show that the theoretical suppression of the Zeno effect can be simply interpreted in terms of the emergence of a classical random walk for the exciton dynamics. In this limit, we show that the quantum master equation becomes a simple classical Fokker-Planck equation, whose diffusivity tensor is given by the coupling-coupling correlation matrix. Furthermore, in section 3 we show that slow frequency components at the limits of validity of the HSR approach are present in specific cross-correlations. In section 4 we use an original elastic network model approach to rationalize the emergence of these low frequencies in terms of specific collective modes involving preferentially the subnetwork of cysteines that are covalently linked to the pigments. In section 5 we epitomize our results, discussing critically HSR based approaches and

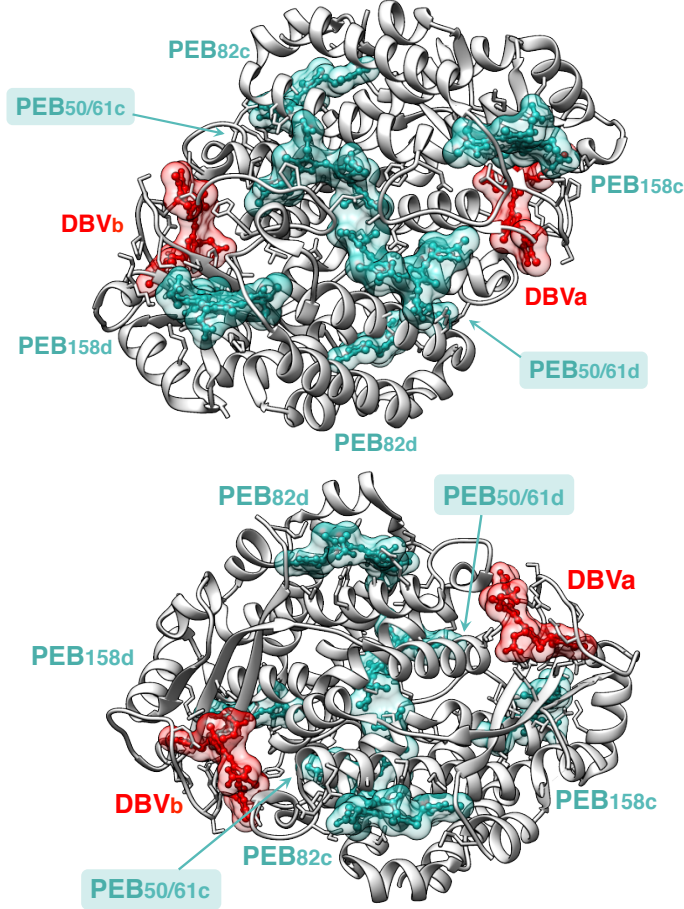


Figure 1. The structure of the PE545 light-harvesting complex (dimer) with the eight light-absorbing pigments (bilins) shown explicitly. There are two types of bilins in the complex: dihydrobiliverdins (DBV) and phycoerythrobilins (PEB). Both are linear molecules consisting of four pyrrole rings (tetrapyrroles). All the eight pigments are covalently linked to the protein scaffold by relatively stable thioether bonds involving specific Cysteines in the protein matrix [29]. The central pair of highly correlated PEB pigments is highlighted. Top: front view with the PEB50/61 pair in the front. Bottom: rear view with the PEB50/61 pair in the back.

suggesting an alternative way to dissect the fold-rooted spatiotemporal signatures of exciton transport in light-harvesting structures based on elastic network models.

2. Reduced quantum master equation from QM/MM simulations

The excitonic two-level system consisting of $N = 8$ pigments of the light-harvesting complex can be described by the tight-binding Hamiltonian given by

$$H_0 = \sum_{m=0}^{N-1} \epsilon_m |m\rangle\langle m| + \sum_{n<m}^{N-1} J_{mn} (|m\rangle\langle n| + |n\rangle\langle m|) \quad (1)$$

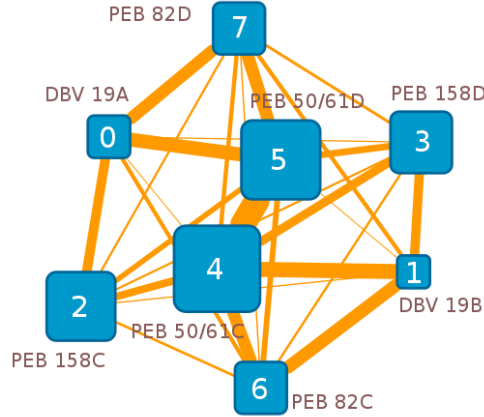


Figure 2. The exciton network corresponding to the Hamiltonian H of the PE545 light-harvesting antenna according to the parameters reported in Ref. [12]. The sizes of nodes and edges account for the amplitude of average pigment site-energies and couplings, respectively. The spatial arrangement of nodes reflects the position of chromophores in the complex, see Fig. 1, rear view. In particular, the two central PEBs (50/61) appear clearly to form the most *connected* pair in the system.

where the state $|m\rangle$ denotes an electronic excitation localized on chromophore m . The site energies and pigment-pigment couplings are given by ϵ_m and J_{mn} respectively. For the parametrization of the Hamiltonian H_0 of the bilin system we refer to [12], see also the online supporting information. The associated network is shown in Fig. 2, where we identify the nodes of the network from $m = 0$ to $m = N - 1 = 7$ with the eight bilin molecules of the complex and (weighted) links represent the associated coupling strengths. To include the effect of a thermally fluctuating environment, the original approach of Haken and Strobl [15, 16] requires one to solve a modified problem, described by the Hamiltonian

$$H(t) = H_0 + h(t) \quad (2)$$

where the Hermitian operator $h(t)$ is a time-dependent perturbation of the Hamiltonian H_0 , whose temporal evolution reflects the bath dynamics. In this framework, the so called Haken-Strobl-Reineker model [16, 14] assumes that the environmental fluctuations $h(t)$ are classical Gaussian Markovian processes with zero average and correlations given by

$$C_{mnpq}(t - t') \equiv \langle h_{mn}(t)h_{pq}(t') \rangle = 2\delta(t - t')\Gamma_{mnpq} \quad (3)$$

where the four-indices tensor Γ_{mnpq} is invariant under the following set of index permutations [14]

$$(mn) \rightarrow (nm) \quad (pq) \rightarrow (qp) \quad (mnpq) \rightarrow (pqmn) \quad (4)$$

With the above hypotheses, the information on the external environment is fully encoded in the tensor Γ_{mnpq} .

Finally, to account for the exciton losses due to internal recombination processes and exciton transfer to the reaction center, we add to the system Hamiltonian H_0 an anti-Hermitian operator defined as

$$iH_d = -i\hbar \sum_m (\alpha_m + \kappa_m) |m\rangle\langle m| \quad (5)$$

In the above formula, α_m and κ_m are the site-dependent recombination and trapping rates, respectively. Altogether, it can be shown [16] that the evolution of the density matrix of the system is described by the following master equation

$$\begin{aligned} \frac{d\rho_{nm}}{dt} = & -i [H_0, \rho]_{nm} - i [H_d, \rho]_{nm}^+ \\ & + \sum_{pq} (2\Gamma_{npqm}\rho_{pq} - \Gamma_{nppq}\rho_{qm} - \Gamma_{pmqp}\rho_{nq}) \end{aligned} \quad (6)$$

where the symbols $[\cdot, \cdot]$ and $[\cdot, \cdot]^+$ denote the commutator and the anti-commutator respectively. The first term in the r.h.s of Eq. (6) describes the unitary part of the evolution, the second one incorporates the dissipative effects defined in Eq. (5), while the third one accounts for the action of the incoherent noise.

Following Vlaming and Silbey [14], it is instructive to single out three physically different types of elements of the tensor Γ , namely:

- (i) Site energy-site energy correlations, Γ_{mnnn}
- (ii) Site energy-coupling correlations, Γ_{mmpq} with $p \neq q$
- (iii) Coupling-coupling correlations, Γ_{nmpq} with $n \neq m$ and $p \neq q$

In the following subsection we will discuss how to estimate the bath tensor Γ directly from atomic-level QM/MM simulations.

2.1. Microscopic description of the exciton environment

All the excitonic parameters (site energies and excitonic couplings in $H(t)$, see Eq. (2)) have been calculated with a polarizable quantum mechanical/molecular mechanical (QM/MMPol) methodology [30] using a trajectory obtained with a ground-state classical MD simulation of PE545 in water (see Ref. [22] for more details). In particular, we extracted 60000 snapshots every 5 fs corresponding to 300 ps of a MD simulation of PE545 for the subsequent QM/MMPol calculations. Because of the considerable computational cost involved in the QM/MMPol calculations, we adopted the ZINDO semi-empirical method [31] to describe the excited states of the pigments, whereas the protein and the solvent were described using a polarizable force field. All details about the QM/MMPol model are reported in Refs [12] and [22]. A detailed study on the parametrization of H_0 for PE545 is contained in Ref. [12]. Concerning the environment fluctuations described by the term $h(t)$, the white noise approximation of the HSR model, Eq. (3), assumes that the bath degrees of freedom decorrelate much faster than the typical exciton timescales. Therefore, in this limit, one can formally integrate Eq. (3), writing

$$2\Gamma_{mnpq} = \int_{-\infty}^{+\infty} C_{mnpq}(\tau) d\tau \quad (7)$$

where it clearly appears that Γ_{mnpq} are related to the zero-frequency limit of the Fourier transform $C_{mnpq}(\omega)$. Notice that, despite the integration up to arbitrarily large times in the above formula, the relevant contribution of correlations to the tensor Γ is expected to come exclusively from very short times. An instructive example is offered by the case of an exponential decay of the correlation function, $C(\tau) = C(0) \exp(-|\tau|/\tau_c)$, which gives $\Gamma = C(0)\tau_c$. In this example τ_c defines the characteristic timescale of bath correlations, so that the contribution to the integral in Eq. (7) for times $|\tau| \gg \tau_c$ is exponentially small in τ .

By means of Eq. (7), we have computed the elements of the tensor Γ_{mnpq} from the environment correlation functions C_{mnpq} extracted from QM/MM trajectories. An effective infrared threshold Θ was imposed, in order to exclude the contribution of slow environmental correlations which are inconsistent with the HSR white-noise approximation of the exciton-protein coupling dynamics. Accordingly, in Eq. (7) we have neglected the correlations displaying a decaying time $\tau_c > \Theta$ (see the supplemental material for further details).

The choice of Θ is a rather delicate point, since on the one hand Θ should be taken as small as possible for the Markovian approximation to hold, on the other the limit $\Theta = 0$ yields vanishing couplings Γ_{mnpq} , thus washing out the whole environment in the HSR description. A detailed study of the optimal choice of Θ for the description of the PE545 protein environment is beyond the scope of the present paper. Here, we take a pragmatic approach by focusing on the upper bound of Θ , that is set by the intrinsic excitonic timescales. In particular, we have chosen $\Theta = 1$ ps, which is comparable to the typical exciton transfer timescales found in Ref. [12] for the PE545 complex. An analysis of the role of Θ for the amplitude of the HS coefficients is provided at the end of Section 3.

3. HSR coefficients: the white noise approximation

An overall view of the relevant Haken-Strobl couplings obtained with this method provided in Fig. 3, where we separately plot the elements of kind i, ii and iii up to the permutations stated in Eq. (4). Here, in order to represent unambiguously the elements Γ_{mnpq} , we have introduced an octal integer w ranging from 0 to 7777, whose digits are $mnpq$. For each sector, we therefore plot the nonvanishing coefficients Γ_w . Consistently with other studies [11], we find that the relevant contribution (order 100 cm^{-1}) in the tensor Γ_w is given by the diagonal terms γ_{mmmm} in sector i . Notice however that these terms display a clear dependence on the pigment site m with an approximate correlation induced by the global geometry of the complex, as also emphasized in Ref. [26] – see for instance the two lowest terms Γ_{6666} and Γ_{7777} , which correspond to “antipodal” pigments PEB 82C and PEB 82D in Fig. 1. Still within sector i , we have found no relevant contributions from site-energies cross correlations, i.e. Γ_{mmnn} with $m \neq n$. This is consistent with a previous study by Schulten *et al.* for the FMO complex [32] and reinforces the idea that in general fluctuations in the excitation energies on different pigments are not significantly correlated on the time scales of exciton transfer. Concerning sector ii correlations, the maximum amplitude of Γ_w is of order 1 cm^{-1} in absolute value. Moreover, we find that large couplings typically correspond to anticorrelations (i.e. negative Γ_w) between the site energy of a pigment m and a coupling involving *the same* pigment m , i.e. for $w = mmmm$ or $w = mmmn$ with $m \neq n$. This last property was already spotlighted in Ref. [33] from the analysis of static correlation functions. A more detailed presentation of the

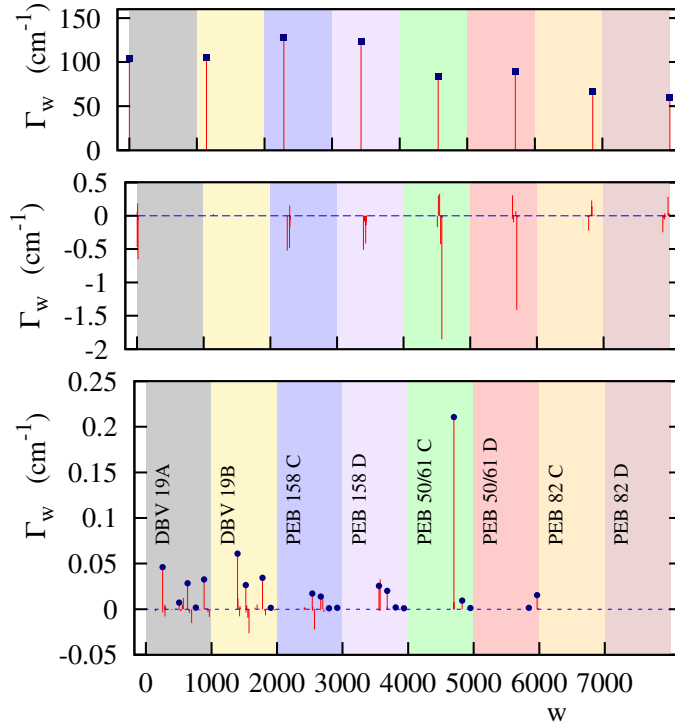


Figure 3. Bath parameter Γ_w extracted from QM/MM simulations at $T = 300K$. The index w is the octal representation of the number $mnpq$. Upper panel: site energy autocorrelation terms of type Γ_{mmmm} (sector ii); central panel: site energy-couplings correlations of type Γ_{mmpq} with $p \neq q$ (sector ii); lower panel: Coupling-coupling terms of type Γ_{mnpq} , with $m < n$, $p < q$, $m \leq p$, $n \leq q$ (sector iii). Blue dots represent coupling autocorrelations, i.e. terms Γ_{mnmn} . Each colored stripe delimits all the possible combinations of the kind $mnpq$ for each pigment index m .

environment couplings in sector ii is provided in the supplemental material.

Here, we observe that the largest couplings that emerge in this sector are $\Gamma_{4445} = -1.8 \text{ cm}^{-1}$ and $\Gamma_{5545} = -1.4 \text{ cm}^{-1}$ (see the central panel of Fig. 3). These correspond to the correlations between the site energies and the coupling of the strongly-interacting central pair of pigments PEB 50/61C and PEB 50/61D, see Fig. 2. It is therefore not surprising that all the other couplings in sector ii are significantly smaller than these two ones. Moreover, according to the analytical results found by Chen and Silbey [13] in the HSR model, environment couplings in sector ii are expected to trigger population oscillations depending on the difference $\Gamma_{mnmn} - \Gamma_{nnmm}$. Since the relevant terms Γ_{4445} and Γ_{5545} have the same sign and comparable absolute amplitude, we do not expect any relevant phenomenon related to long-lived oscillations in the HSR approximation.

Moving finally to sector iii , Fig. 3 shows that the amplitude of all Γ_w falls below 0.1 cm^{-1} except for the term Γ_{4545} which is representative of the coupling autocorrelations of the central couple of pigments. More generally, we find that the non-vanishing terms in this sector typically correspond to coupling autocorrelations,

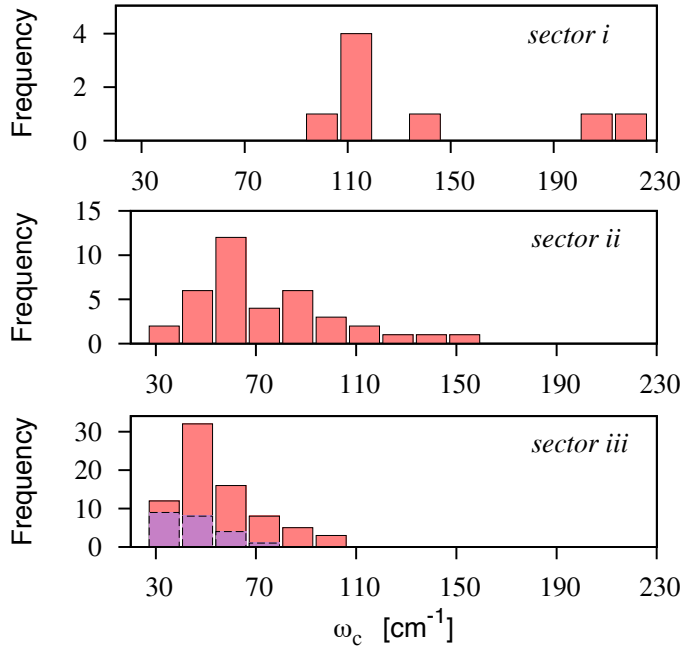


Figure 4. Histograms of the spectral widths ω_c extracted by fitting a Lorentzian line shape to the cosine Fourier transforms of the autocorrelation functions $C_{mnpq}(\omega)$ in the range $[0, 500]$ cm^{-1} . The three panels show the distribution of ω_c in each correlation sector. For sector *iii* the purple bars refer to coupling-coupling autocorrelations, i.e. to $C_{mnmn}(\omega)$ with $m \neq n$. Histograms are computed for $\omega_c \geq 2\pi/\Theta \simeq 33$ cm^{-1} .

in the form Γ_{mnmn} with $m \neq n$, (see the blue dots in Fig. 3). On the other hand, coupling cross correlations Γ_{mnpq} with $m \neq n$, $p \neq q$ and $mn \neq pq$ provide a marginal contribution to sector *iii*, typically of the order of 10^{-3} cm^{-1} .

A complementary view on the extracted coefficients Γ_{mnpq} can be obtained by formally estimating a time scale for the decay of the associated time correlations. In the simplest hypothesis of a single finite time decay constant, one should replace eq. (3) by

$$C_{mnpq}(t-t') \equiv \langle h_{mn}(t)h_{pq}(t') \rangle = \frac{2e^{-|t-t'|/\tau_c}}{\tau_c} \Gamma_{mnpq} \quad (8)$$

Accordingly an estimate of the spectral width $\omega_c = 2\pi/\tau_c$ can be obtained from the QM/MM data by consistently fitting a Lorentzian to the cosine Fourier transform of the correlation functions. Fig. 4 displays the result of this analysis for each sector. While site energy autocorrelations (sector *i*) display a fast decay, correlations in sectors *ii* and *iii* decay with timescales that are comparable with the typical exciton timescales [12]. More precisely, we find the following ordering with respect to average decreasing ω_c : site-energy autocorrelations, site-energy-coupling correlations, couplings cross correlations, coupling autocorrelations. This analysis proves that coupling-coupling autocorrelations lie at the limits of validity of the white-noise approximation intrinsic to the HSR approach. In this sense, exciton transport in

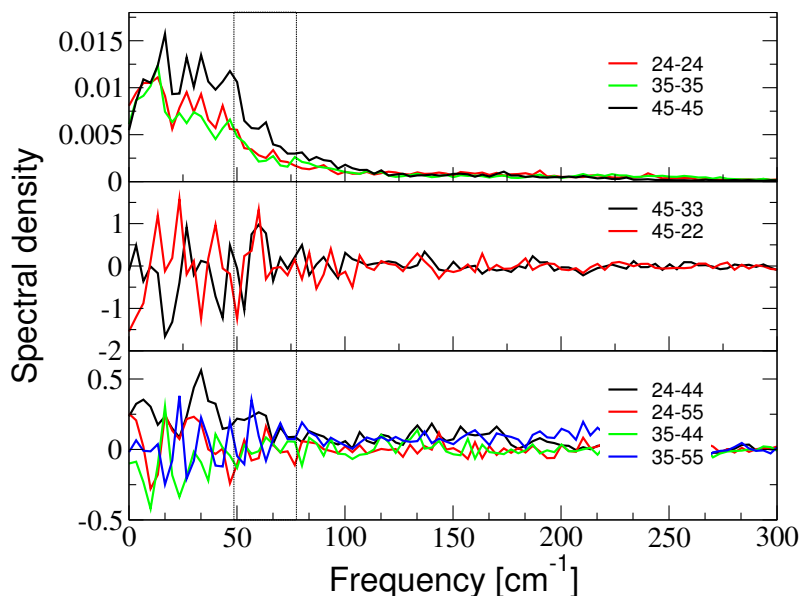


Figure 5. Cosine Fourier transform of selected auto and cross correlation functions. For example, the black and red lines in the middle panel refer to the cross correlations between the fluctuations of the PEB50/61C-PEB50/61D coupling (45) and the PEB158D (3) and PEB158C (2) site energies, respectively. The numbering of pigments is the one illustrated in Fig. 2. The vertical dashed lines delimit the frequency region where our ENM analysis identify normal modes expressing concerted motions of the sub-network of CYS residues covalently linked to the pigments through disulfide bridges (see text). The spectra in the upper panel have been normalized to unit area for the sake of clarity. The others have units of cm.

proteins would possibly require more sophisticated methods such as used in organics semiconductors, where it is known that coupling-coupling fluctuations are dominated by low-frequency, collective vibrations of the molecular crystal [34, 35, 36]. More precisely, in the case of the PE545 protein it turns out that signatures of slow frequency components emerge in the correlations among selected coupling and/or site energy fluctuations. A few typical examples illustrating this behaviour are reported in Fig. 5. Fluctuations with frequencies of the order of a few tens of cm^{-1} are likely to flag low-frequency, collective normal modes (NM) of the protein matrix, which could potentially spotlight important, fold-rooted motions expressed by the protein scaffold with the aim of selectively promoting transport by helping break localization of exciton wavefunctions induced by disorder in the site energies [37, 4]. In section 4 we shall dig further into this hypothesis, with the aim of uncovering whether the PE545 protein structure is indeed able to express specific, potentially functional, transport-enhancing normal modes in the highlighted frequency range. In the next section, we stick to the white-noise approximation and turn to investigate the effect of the QM/MM-based correlations on exciton transport.

3.1. Exciton transfer efficiency

The exciton transfer process can be quantified by means of two simple indicators, namely the transfer efficiency η and the average transfer time \bar{t} [4]. These quantities can be computed simply in terms of time evolution of the one-exciton density matrix,

$$\eta = 2 \sum_m \kappa_m \int_0^\infty dt \langle m | \rho(t) | m \rangle \quad (9)$$

$$\bar{t} = \frac{2}{\eta} \sum_m \kappa_m \int_0^\infty dt t \langle m | \rho(t) | m \rangle \quad (10)$$

The presence of a finite recombination rate α_m in Eq. (5) introduces a non-specific channel for exciton losses, that reduces the energy flux towards the specific trapping site. Therefore, the efficiency parameter $\eta \in [0, 1]$ quantifies the probability that an exciton is successfully driven to the trap before it recombines. A typical value of α_m is estimated to be independent of m and of order 1 ns^{-1} [4]. On the other hand, we assume the presence of a single trapping site located on the lowest-energy pigment ($m = 1$) (*DBV_{19B}*) [12] with trapping rate of 1 ps^{-1} . In order to explore the role of environment fluctuations in Eq. 6, we introduce a linear dependence of Γ_w on the system temperature T , namely $\Gamma_w(T) = (T/T_r)\Gamma_r$ where $T_r = 300 \text{ K}$ denotes room temperature and Γ_r is the coupling tensor at $T = T_r$ computed from QM/MM simulations as discussed in Section 3.

In Fig. 6 we show the parameters η and \bar{t} as a function of temperature for an exciton initially localized on pigment PEB50/61D (site $m = 5$), i.e. one of the bilins forming the central pair of strongly interacting pigments (see Fig. 2). Similarly to previous studies on the FMO complex [4], we find that at room temperature $T = T_r$, the PE545 complex has almost reached the condition of maximum efficiency and minimum transfer time. Moreover, this quasi-optimum condition is by all practical means rather insensitive to temperature (note the logarithmic scale on the x -axis) in a range of temperatures where there can be safely asserted that the protein is in its folded, fully functional structure. It is worthwhile to observe that this temperature range is rather narrow, typically $\pm 50 \text{ K}$ around room temperature. It is evident from Fig. 6 that the efficiency and average transfer times are rather constant in this temperature range (see vertical dashed lines in the top panel). It should be reminded that, strictly speaking, it is meaningless to consider exciton transport in light-harvesting systems outside this temperature range.

In order to gain a deeper insight on the overall transport phenomenon, we have repeated the same numerical experiment by selectively “silencing” parts of the dynamical contributions appearing in Eq. 6. A first important result is that, for the wide range of temperatures here considered (biologically relevant and irrelevant), negligible variations are observed upon neglecting all the possible cross-correlations in Γ_w (see cyan triangles in Fig. 6). This suggests that cross correlations in sectors *ii* and *iii* do not play a relevant role for the transport properties of the bilin complex. A complete definition of HSR coupling parameters in the limit of vanishing cross correlations is provided in the supplemental material. Further insight can be gathered from a further reduction of Γ_w to a diagonal tensor with non-vanishing elements of kind Γ_{mmmm} , i.e. the coefficients shown in the upper panel of Fig. 3. The above approximations lead to the usual description of environmental effects in terms of *pure dephasing* noise, where optimal transport was shown to emerge [4] for a *finite* dephasing rate. It is clear from Fig. 6 that the characteristic high-temperature efficiency drop

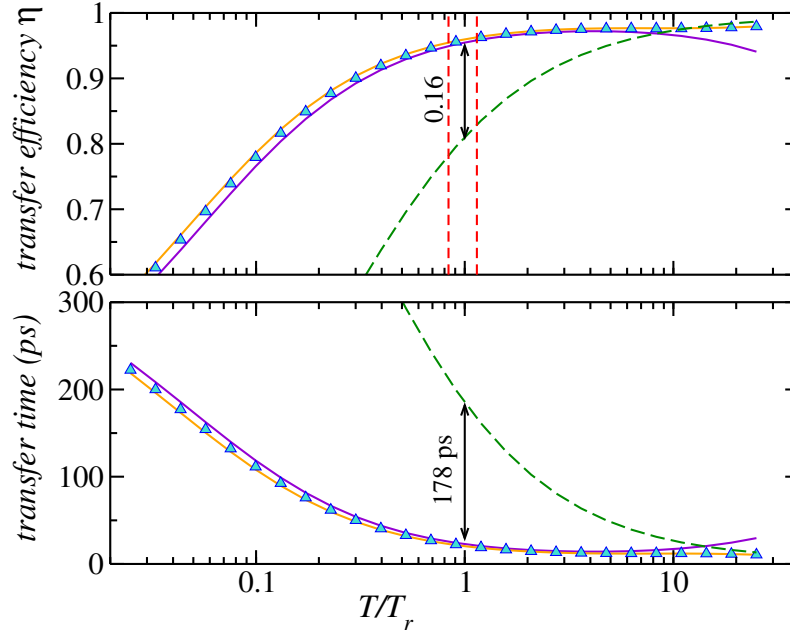


Figure 6. Exciton transfer efficiency (top) and average transfer time (bottom) as a function of temperature for the exciton Hamiltonian H_0 . The purple curve refers to the evolution where only site energy fluctuations are allowed (pure dephasing noise). The orange curve accounts for the dynamics in Eq. 6 with the full tensor Γ_w shown in Fig. 3, while cyan triangles are obtained considering only site energy autocorrelations and coupling autocorrelations. The green dashed line shows the result obtained from a purely incoherent population transfer, see Eq. (11). The arrows identify the differences between the quantum and classical (purely incoherent) models at room temperature, while the vertical dashed lines in the top panel identify the typical stability region of proteins, $(240 \pm 17 < T < 343 \pm 14)$ K [38]. Simulations refer to dissipation rates $\alpha_m = \alpha = 1 \text{ ns}^{-1}$ and $\kappa_m = \kappa \delta_{1,m}$ with $\kappa = 1 \text{ ps}^{-1}$.

(associated in Ref. [4] with the quantum Zeno effect [27]) is no longer present when generalized correlations beyond pure dephasing are considered. This result is a direct consequence of the presence of small but non-vanishing coupling fluctuations, i.e. of terms Γ_{mnmn} with $(m \neq n)$, which promote a population transfer between sites m and n [15, 16, 13, 14]. A similar effect was recently observed in Ref. [28, 39] within the framework of an explicit nonlinear quantum-classical hybrid model. As a general observation, we emphasize that the Zeno-like decrease in efficiency associated with pure dephasing falls in a temperature range where the protein matrix would be in a wildly denatured state, which means that such regime is by all means not biologically relevant and could not have been possibly accessed by evolution. We observe that this conclusion would hold *a fortiori* were the mapping between temperature and strength of correlations nonlinear, i.e. $\Gamma_w(T) = (T/T_r)^\nu \Gamma_r$ with $\nu > 1$.

The high-temperature regime can be captured by a simple master equation for purely incoherent population transfer (a classical random walk) in the form

$$\frac{d\rho_{nn}}{dt} = \sum_{m \neq n} \Gamma_{nmnm} \rho_{mm} - \rho_{nn} \sum_{m \neq n} \Gamma_{nmnm} \quad , \quad (11)$$

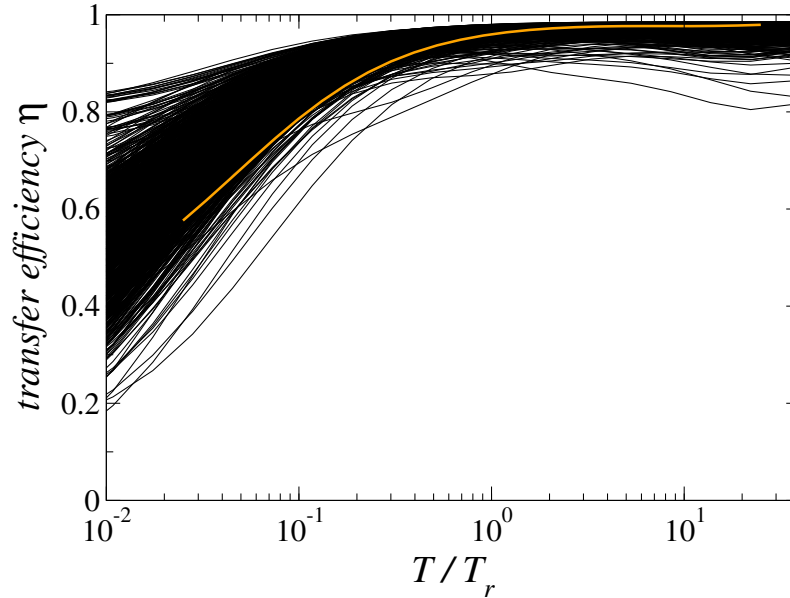


Figure 7. Exciton transfer efficiency as a function of temperature for different modified Hamiltonians obtained by randomly reshuffling the off-diagonal elements J_{nm} of H_0 (see Eq. (1)) and the corresponding QM/MM fluctuations (corresponding to coupling-coupling autocorrelations). Simulations refer to 1000 independent reshufflings. Other parameters were set as in Fig. 6. The orange line denotes the results shown in Fig. 6 obtained with the full tensor Γ_w shown in Fig. 3.

where only coupling autocorrelations are considered (see green dashed line in Fig. 6). Eq. (11) is essentially a Fokker-Planck equation for the classical occupation probability ρ_{nn} on pigment n . As shown in Fig. 6, the purely classical description approaches the generalized HSR dynamics in the region $T \gtrsim 10 T_r$. It is worth noting that the purely diffusive description underestimates the transfer efficiency by about 17 % (and correspondingly overestimates the average transfer time of a larger factor of about 8) in the biologically relevant temperature region (see arrows in Fig. 6), suggesting that some degree of coherence is indeed important to achieve optimal transport.

From the previous analyses it is clear that a certain amount of noise is required to break disorder-induced localization of the exciton caused by the heterogeneity of local site energies. An interesting question to ask is what is the role of the specific *realization* of such noise, in terms of the correspondence between the elements of the tensor Γ_{mnpq} and specific pairs of pigments in the structure. One simple way to address this question is to investigate the effect on transport of randomly reshuffling the the tensor elements. For this purpose, one can restrict to site-energy and coupling-coupling auto-correlations (it is clear from Fig. 6 that this will not induce appreciable differences on the results). In terms of the associated tight-binding network (see Fig. 2), this amounts to randomly rewiring the nodes. Fig. 7 shows efficiency curves computed for a large number of independent random rewiring realizations. Each of this corresponds to a different random reshuffling of the pairs (J_{nm}, Γ_{nmnm}) , with $n \neq m$, i.e. pigment couplings and associated pigment-pigment noise. It is clear that in the

physically relevant region close to Γ_r , deviations from the efficiency corresponding to the *true* set of physical parameters are negligible. Analogous results were obtained when considering random reshufflings of site energies and associated noise terms, i.e. the pairs (J_{mm}, Γ_{mmmm}) , or combinations of both strategies. Moreover, deviations of the same order of magnitude were obtained for the corresponding average transfer times (results not shown).

Overall, this analysis seems to suggest that high transport efficiency in a tight-binding model with site disorder can be achieved robustly through noise, rather insensitively of the specific connectivity pattern of the tight-binding network. At the same time, one should be warned that efficiency is a rather *global* indicator. Therefore, some caution is required in interpreting this result as a thorough dismissal of tight and specific connections between the physical and geometrical structures underlying noise correlations and the propagation of quantum excitations coupled to the vibrating, noise-producing scaffold. Moreover, disregarding explicitly certain slow frequency components in the spectral densities, in accordance with the white noise prescription, could prove a crucial limitation in the quest for quantitative links between protein vibrations and exciton transport. All in all, although descriptions of the HSR type prove that a certain degree of quantum coherence increases quantum efficiency over purely incoherent, hopping transport, one should probably couple these with quantum-classical hybrid methods, where structure-encoded spatiotemporal correlations provide an *explicit* description of noise. In the next section, based on the spectral features emerging from QM/MM correlations in the PE5454 complex, we develop a general method to dig for possible exciton-coupled vibrational patterns of the protein matrix.

4. HSR coefficients: an elastic-network analysis reveals specific low-frequency normal modes

In this section, we consider the question whether the slow-frequency components emerging in certain QM/MM-based spectral densities (see again Fig. 5) flag specific *collective vibrations*, whose pattern is encoded in the protein scaffold and that would selectively couple to exciton transport at the limits of validity of the HSR approach.

The elastic-network model (ENM) denotes a class of powerful and rather inexpensive tools that are well suited to the investigation of collective fluctuations of proteins [40, 41, 42, 43, 44]. In the residue coarse-grained (CG) version, also known as the anisotropic network model (ANM) [40], the protein is described as a network of as many fictive beads as there are amino acids. In the simplest case, each bead possesses the same mass equal to the average amino acid mass (about 110 a.m.u.) and occupies at rest the position of the corresponding α Carbon along the backbone chain of the protein as determined from an experimentally solved structure, i.e. X-ray or NMR. The beads interact through identical Hooke springs with other beads in the structure located within a specified cutoff distance R_c . According to this prescription, the total potential energy of such elastic network model reads ‡

$$U = \frac{1}{2} k_2 \sum_{i>j=1}^N c_{ij} (r_{ij} - R_{ij})^2 \quad (12)$$

where N is the number of residues, R_{ij} and r_{ij} the equilibrium and instantaneous distances between residues i and j , respectively, and k_2 is the common spring stiffness.

‡ See Ref. [45] for a thorough discussion of alternative schemes.

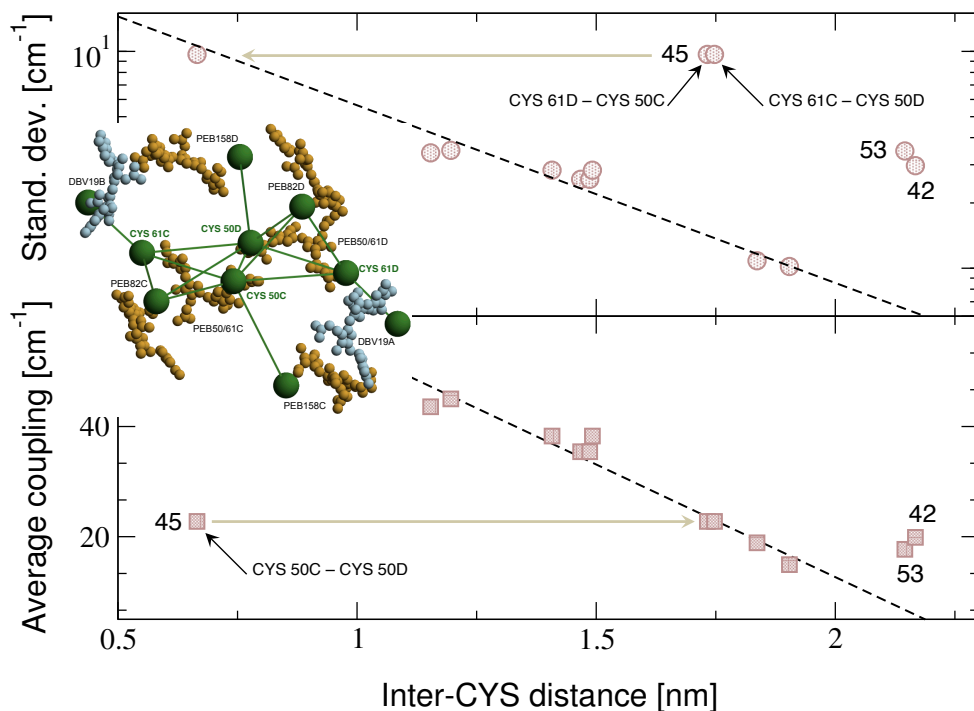


Figure 8. Average absolute value (bottom) and standard deviation (top) of the QM/MM coupling time series versus distance between the covalently attached cysteine residues. The dashed lines are plots of the apparent *typical* trends, namely the exponential decay $\sigma(d) = \sigma_0 \exp(-d/d_\sigma)$, with $\sigma_0 = 37.21 \text{ cm}^{-1}$, $d_\sigma = 5.3 \text{ \AA}$ (top) and $\langle J(d) \rangle = J_0(1 - d/d_c)$, with $J_0 = 94.4 \text{ cm}^{-1}$, $d_c = 23.1 \text{ \AA}$. The cartoon shows the sub-network of covalently attached cysteine residues and the links flag the shortest 15 CYS-CYS inter-distances, from the closest pair, namely CYS 50C and CYS 50 D (6.65 \AA), to the pair CYS158C-CYS50C (21.67 \AA). The couplings that appear to be outliers with anomalously large fluctuations and off-trend average couplings are explicitly highlighted (the numbering is the same as the one used in Fig. 2). **53**: CYS 50D-CYS 158 D, **42**: CYS 50C-CYS 158D.

The matrix c_{ij} specifies the connectivity of the network, namely $c_{ij} = \{1 \text{ for } R_{ij} \leq R_c | 0 \text{ otherwise}\}$. Consensus choices for the two parameters of such a model are $k_2 = 5 \text{ kcal/\AA}^2$ and $R_c = 10 \text{ \AA}$ [46]. The normal modes can be easily computed as the eigenvectors of the Hessian matrix of the potential energy function (12) [47]. With this choice of the parameters, the coarse-grained NM spectrum of PE545 (PDB id. 1XG0) spans the frequency interval [3.9 – 93.5] cm^{-1}

All chromophores in the PE5454 complex are covalently linked through disulfide bridges to specific cysteine residues (CYS) [23]. The central pigments PEB50/61C and PEB50/61D form two disulfide bridges each, while all the other bilins are covalently linked to one cysteine residue each. Overall, these residues form an extended subnetwork of anchor points, whose concerted motions are likely to influence the coupling and site energy fluctuations of the attached pigments. It is instructive to investigate how the average and the standard deviation of the QM/MM coupling time

series depend upon the distance between the respective covalently linked CYS pairs. The data reported in Fig. 8 suggest that on average both indicators referring to a given pair of pigments decrease with the distance between the associated CYS anchor points (dashed lines). Interestingly, pairs associated with slow frequency components in the corresponding spectral densities (see Fig. 5) stand out from the common average trend as outliers. More precisely, fluctuations (gauged here by the standard deviations) of the 53 and 42 pairs are seen to be anomalously large as compared to the average trend at the same CYS-CYS distances. This is all the more remarkable as it concerns pairs located at large distances. Another interesting observation is that the average coupling of the central PEB pair (45) appears to be on the common trend only when associated with pairs of opposite cysteines (61C-50D and 61D-50C, see again the cartoon and the arrow in the bottom panel of Fig. 8). However, this is no longer true for the corresponding fluctuation, which appears to be of the correct order of magnitude only when associated with the two central cysteines (50C-50D, top horizontal arrow). Overall, this suggests that the fluctuations in the 54 coupling are controlled by the relative motions of the CYS50C-CYS50D pair. In turn, this points to the interaction between the associated terminal pyrrole rings (nearly parallel and about 5 Å away from each other) as the main structural unit controlling the fluctuations of the 45 coupling strength.

The above observations strongly suggests that there exist a subset of normal modes in the 30 – 80 cm⁻¹ range whose displacement field (pattern) represents specific concerted motions of the cystein subnetwork. Such modes, showing up in the spectral density referring to specific coupling-coupling and coupling-site energy (cross) correlations, are good candidates in the quest for fold-encoded, transport-enhancing vibrations. In order to identify these modes, we have proceeded as follows. First, we have ranked normal modes in descending order with respect to their involvement fraction on the CYS subnetwork. Let us denote the latter as \mathcal{S}_{cys} and let $\vec{\xi}_i^k$ denote the displacement of particle (residue) i in the mode k . NMs patterns are normalized, i.e. $\sum_{i=1}^{3N-6} |\vec{\xi}_i^k|^2 = 1 \forall k$, so that the quantity

$$f_k = \sum_{i \in \mathcal{S}_{\text{cys}}} |\vec{\xi}_i^k|^2 \leq 1 \quad (13)$$

gauges the relative weight of the covalently linked cysteines in the overall displacement field of the k -th NM. If only those residues were vibrating in a given mode m , one would have $f_m = 1$.

It would be tempting to rank all normal modes in descending order with respect to the associated f_k values and select the top-scoring ones. However, a moment's thought is enough to realize that one also needs to gauge the *statistical significance* of a given f_k score. This should be done by considering for each mode the null hypothesis that a totally random subset of as many residues would give the same score. Thus, for each NM we have computed a p -value by performing a large number $N_R = 10^4$ of random reshufflings of the NM pattern and computing the corresponding value of the involvement score $f_k^R(i), i = 1, 2, \dots, N_R$. The statistical significance of the measured involvement for a given NM can then be estimated by the fraction of random scores exceeding the measured one. Namely,

$$p_f = \frac{1}{N_R} \sum_{i=1}^{N_R} \Theta(f_k^R(i) - f_k) \quad (14)$$

Table 1. Values of μ_{ij} for different pairs in the CYS-CYS subnetwork for the 8 normal modes with $p_f, p_\mu < 0.05$. The figure $\bar{\mu}$ is the average value over the considered 15 pairs (see text). The last column reports the μ -confidence level (c.l.), i.e. $1 - p_\mu$. Normal modes are numbered starting from the highest frequency one.

NM	ω [cm ⁻¹]	$\bar{\mu}$	50C-50D	61D-50C	50D-61C	158D-50D	158C-50C	c.l.
144	77.49	0.639	-0.915	-0.750	0.888	0.251	0.386	0.974
245	72.45	0.691	0.866	1.000	-0.659	0.215	-0.974	0.995
432	65.74	0.636	-0.706	0.475	-0.770	-0.380	-0.585	0.972
501	63.37	0.639	0.900	-0.901	-0.478	0.904	0.750	0.971
531	62.39	0.635	0.731	0.994	-0.853	-0.605	0.146	0.963
546	61.87	0.764	-0.991	0.317	0.634	-0.980	0.850	1.000
556	61.50	0.650	0.402	-0.814	0.965	-0.505	0.652	0.976
940	48.57	0.623	0.941	0.104	0.904	0.927	-0.669	0.953

where $\Theta(x)$ is Heaviside function. The quantity $1 - p_f$ gauges the rejection probability of the null hypothesis. If we restrict to confidence levels greater than 95 %, this analysis singles out 78 NMs with frequencies lying between $\omega_1 = 31.98$ cm⁻¹ and $\omega_2 = 77.49$ cm⁻¹, i.e. 6.9 % of the NMs in the same frequency range and 5.3 % of the total number of NMs. We term this ensemble \mathcal{M}_{95} . Interestingly, this is precisely the same frequency range where low-frequency structures appear in specific spectral-densities (see again Fig. 5). It is possible to refine further the choice of possible interesting NMs by isolating vibrations whose vibrational patterns are mostly directed along the directions joining pairs of cysteines in the covalent subnetwork. We isolated the closest 15 pairs, which correspond to two links in the connectivity graph ($R_c = 10$ Å, inter-distances shorter than 21.67 Å, see cartoon in Fig. 8). For each NM we computed the projection

$$\mu_{ij}^k = \frac{\vec{\xi}_i^k - \vec{\xi}_j^k}{\left\| \vec{\xi}_i^k - \vec{\xi}_j^k \right\|} \cdot \hat{R}_{ij} \quad (15)$$

where \hat{R}_{ij} denotes the unit vector joining cysteine i to cysteine j in the equilibrium structure. Again, one needs to evaluate the rejection probability of the null hypothesis stipulating that a value of μ equal or higher than a measured one can be obtained by selecting 15 random pairs of residues in the entire structure. We then considered the NMs in the previously identified subset \mathcal{M}_{95} and computed the indicators μ_{ij}^k and their associated p -values, defined as

$$p_\mu = \frac{1}{N_R} \sum_{i=1}^{N_R} \Theta(\bar{\mu}^R(i) - \bar{\mu}^k) \quad (16)$$

where $\bar{\mu}$ refers to the average of the projections (15) computed over the 15 closest cysteine pairs ($\bar{\mu}^k$) and over as many randomly selected pairs ($\bar{\mu}^R$) for a given normal mode k in the subset \mathcal{M}_{95} .

Remarkably, 10 % of these modes (8 NMs out of 78) showed a confidence level $1 - p_\mu$ greater than 95 %. A summary of this analysis is reported in Table 1. Such

modes have frequencies in a somewhat narrower range than the previous 78 ones, lying in the range $[48.57, 77.49]$ cm^{-1} (see vertical lines in Fig. 5). The average projection on the first 15 CYS-CYS inter-distances over the whole subset is 0.66, suggesting that these NMs are indeed concerted motions of the CYS-CYS subnetwork, whose vibrational patterns can be imagined to a great extent as acting along the links of the associated connectivity subgraph (see green sticks in the cartoon in Fig. 8). Remarkably, the average projection μ_{ij} on the 50C-50D direction (corresponding to the largest QM/MM coupling fluctuation) is 0.81, larger than the average projection computed for all the 15 pairs. This strongly confirms our previous inference about the crucial role of these two cysteines in mediating the protein-encoded fluctuations that couple to exciton transport.

5. Conclusions and perspectives

In this paper we have provided a realistic parametrization of the Haken-Strobl model (6) for the PE545 bilin complex from QM/MM simulations. The aim of our analysis was to dig for the different auto- and cross-correlations relating to pigment site energies and pigment-pigment couplings and investigate their role on exciton mobility. We have used this approach to characterize exciton transport by means of simple global observables, namely the transport efficiency and the average transfer time. As a result, we have obtained that at room temperature the system is very close to the optimal transport regime with a predominant contribution from site-energy fluctuations. Moreover, in the optimal regime the transport efficiency is rather insensitive to random reshuffling of the elements of the Hamiltonian and the associated noise tensor. This suggests that noise-induced depinning of quantum excitations in disordered environments is a rather general feature of open quantum systems.

The high temperature regime revealed that the small residual coupling fluctuations in the dynamics suppress the quantum Zeno regime at temperatures $T \gtrsim 5 T_r$, where the dynamics is essentially that of a classical random walk. Although this regime is not meaningful from a biological standpoint, since proteins unfold at temperatures $T \gtrsim 1.2 T_r$, our study provides a different reading frame for noise-assisted quantum transport [4] in photosynthetic complexes. Namely, the effect of environment fluctuations at room temperature is to provide access to *the same* efficiency level that would pertain to an inaccessible regime of classical diffusion at extremely high temperatures. To put it in more evocative terms, one might argue that evolution has taken advantage of the laws of quantum mechanics to lower the effective temperature corresponding to the highest efficiency (the classical regime) to the region of working temperatures of proteins in a living organism.

We have shown that QM/MM data spotlight clear slow frequency components in the $[30-80]$ cm^{-1} range in the spectral densities associated with specific coupling-coupling and coupling-sit energy fluctuations. Typically these involve the central PEB50/61D/C pigments. These lie at the threshold of validity of the white noise approximation inherent in HSR-type approaches, where one has to surmise that the noise spectral structure does not contain slow components, relaxing in time as fast as or more slowly than the timescale associated with exciton transfer.

While there seems to be no obvious way to include slow, collective modes in HSR-kind descriptions of exciton transport, in the last section of the paper we lay out a possible strategy to tackle this problem through the elastic-network model formalism. Our analysis clearly identify a set of specific collective normal modes that preferentially

couple the subnetwork of 10 cysteine residues covalently linked to bilins. Such modes, selected through an original double statistical-significance analysis, have the combined properties of (i) maximum concerted involvement on the CYS subnetwork and (ii) maximum displacement *alignment* with the ensemble of the closest inter-distance vectors between cysteine pairs. These modes, with frequency lying in the [50-80] cm^{-1} range, might be important fold-encoded *noise* sources for enhancing exciton transport optimally within the pigment-hosting protein matrix.

The logical step beyond microscopically parameterized HSR approaches to investigate the above hypothesis is to turn to coarse-grained quantum-classical hybrid descriptions, often also called mixed quantum classical approaches (QCA) [48]. In QCAs the force acting on classical degrees of freedom is computed by considering an effective potential energy given by the quantum mechanical expectation value of the system-reservoir coupling according to the instantaneous values of the classical coordinates and the wave function of the quantum degrees of freedom (DOFs). While the presence of the classical DOFs results in an additional potential for the dynamics of the quantum system, the classical reservoir feels the quantum mechanically averaged force of the relevant quantum system. This method is often referred to as Ehrenfest method [48] and falls within the class of mean-field approaches. Interestingly, a recent QCA based on the nonlinear network model [46] has shown that specific fold-rooted vibrational modes have the potential to spotlight alternative excitation energy transfer routes in the Fenna-Matthews-Olson (FMO) complex through their influence on pigment properties [49]. Overall, also in view of the results of the previous section, elastic/nonlinear-network model-based QCAs can be regarded as optimal tools to investigate the role of specific fold-encoded vibrational modes in exciton transport in light-harvesting complexes.

Acknowledgments

S.P., S.I., Y.O. and F.P. thank financial support from the EU FP7 project PAPETS (GA 323901). S.P. and Y.O. thank the support from Fundação para a Ciência e a Tecnologia (Portugal), namely through programmes PTDC/POPH/POCH and projects UID/EEA/50008/2013, IT/QuSim, IT/QuNet, ProQuNet, partially funded by EU FEDER, as well as project CRUP/CPU CQVibes TC16/14. Furthermore S.P. acknowledges the support from the DP-PMI and FCT (Portugal) through scholarship PD/BD/52549/2014.

References

- [1] van Amerongen H, van Grondelle R and Valkunas L 2000 *Photosynthetic Excitons* (World Scientific)
- [2] Mohseni M, Omar Y, Engel G and Plenio M B (eds) 2014 *Quantum Effects in Biology* (Cambridge University Press)
- [3] Adolphs J and Renger T 2006 *Biophysical journal* **91** 2778–2797
- [4] Rebentrost P, Mohseni M, Kassal I, Lloyd S and Aspuru-Guzik A 2009 *New Journal of Physics* **11** 33003
- [5] Caruso F, Chin A W, Datta A, Huelga S F and Plenio M B 2009 *The Journal of Chemical Physics* **131** 105106
- [6] Plenio M B and Huelga S F 2008 *New Journal of Physics* **10** 113019
- [7] Rebentrost P, Mohseni M and Aspuru-Guzik A 2009 *The Journal of Physical Chemistry B* **113** 9942–9947

- [8] Fassioli F, Nazir A and Olaya-Castro A 2010 *The Journal of Physical Chemistry Letters* **1** 2139–2143
- [9] Nalbach P, Eckel J and Thorwart M 2010 *New Journal of Physics* **12** 065043
- [10] Wu J, Liu F, Shen Y, Cao J and Silbey R J 2010 *New Journal of Physics* **12** 105012
- [11] Renger T, Klinger A, Steinecker F, Schmidt Am Busch M, Numata J and M??h F 2012 *Journal of Physical Chemistry B* **116** 14565–14580
- [12] Curutchet C, Novoderezhkin V I, Kongsted J, Muñoz-Losa Auroraoz-Losa A, Van Grondelle R, Scholes G D and Mennucci B 2013 *Journal of Physical Chemistry B* **117** 4263–4273
- [13] Chen X and Silbey R J 2010 *The Journal of chemical physics* **132** 204503
- [14] Vlaming S M and Silbey R J 2012 *The Journal of chemical physics* **136** 55102
- [15] Schwarzer E and Haken H 1972 *Physics Letters A* **42** 317–318
- [16] Haken H and Strobl G 1973 *Zeitschrift f??r Physik* **262** 135–148 ISSN 14346001
- [17] Huo P and Coker D F 2012 *The Journal of chemical physics* **136** 115102
- [18] Huo P and Coker D F 2011 *The Journal of chemical physics* **135** 201101
- [19] Hwang-Fu Y H, Chen W and Cheng Y C 2015 *Chemical Physics* **447** 46–53
- [20] Roden J J J, Bennett D I G and Whaley K B 2016 *The Journal of Chemical Physics* **144** 245101
- [21] Liu X and Kühn O 2016 *Chemical Physics* **481** 272–280
- [22] Curutchet C, Kongsted J, Muñoz-Losa A, Hossein-Nejad H, Scholes G D and Mennucci B 2011 *Journal of the American Chemical Society* **133** 3078–3084
- [23] Doust A B, Marai C N J, Harrop S J, Wilk K E, Curmi P M G and Scholes G D 2004 *Journal of Molecular Biology* **344** 135–153
- [24] Doust A B, Wilk K E, Curmi P M G and Scholes G D 2006 *Journal of Photochemistry and Photobiology A: Chemistry* **184** 1–17
- [25] Novoderezhkin V I, Doust A B, Curutchet C, Scholes G D and Van Grondelle R 2010 *Biophysical Journal* **99** 344–352
- [26] Viani L, Corbella M, Curutchet C, O'Reilly E J, Olaya-Castro A and Mennucci B 2014 *Physical Chemistry Chemical Physics* **16** 16302–16311
- [27] Misra B and Sudarshan E C G 1977 *Journal of Mathematical Physics* **18** 756–763
- [28] Iubini S, Boada O, Omar Y and Piazza F 2015 *New Journal of Physics* **17** 113030
- [29] Scheer H and Zhao K H 2008 *Molecular Microbiology* **68** 263–276
- [30] Curutchet C, Muñoz-Losa A, Monti S, Kongsted J, Scholes G D and Mennucci B 2009 *Journal of chemical theory and computation* **5** 1838–1848
- [31] Zerner M C 1991 *Reviews in computational chemistry* **2** 313–365
- [32] Carsten Olbrich, Johan Strümpfer, Klaus Schulten U K 2011 *The journal of physical chemistry. B* **115** 758
- [33] Viani L, Curutchet C and Mennucci B 2013 *The journal of physical chemistry letters* **4** 372–377
- [34] Troisi A 2011 *Chemical Society reviews* **40** 2347–2358
- [35] Troisi A and Orlandi G 2006 *Phys. Rev. Lett.* **96** 86601
- [36] Aragó J and Troisi A 2015 *Phys. Rev. Lett.* **114** 26402
- [37] Plenio M B and Huelga S F 2008 *New Journal of Physics* **10** 113019
- [38] Sandeep Kumar , , Chung Jung Tsai § and Ruth Nussinov* § 2003 *Biochemistry* **42** 4864–4873
- [39] Moix J M, Khasin M and Cao J 2013 *New Journal of Physics* **15** 085010
- [40] Atilgan A, Durell S, Jernigan R, Demirel M, Keskin O and Bahar I 2001 *Biophys. J.* **80** 505–515
- [41] Hinsén K, Petrescu A J, Dellerue S, Bellissent-Funel M C and Kneller G R 2000 *Chemical Physics* **261** 25–37
- [42] Micheletti C, Lattanzi G and Maritan A 2002 *J. Mol. Biol.* **321** 909–921
- [43] Tama F, Wriggers W and Brooks III C L 2002 *J. Mol. Biol.* **321** 297–305
- [44] Tirion M M 1996 *Phys. Rev. Lett.* **77** 1905–1908
- [45] Bahar I, Lezon T R, Yang L W and Eyal E 2010 *Annual Review of Biophysics* **39** 23–42
- [46] Juanico B, Sanejouand Y H, Piazza F and De Los Rios P 2007 *Phys. Rev. Lett.* **99** 238104
- [47] Sanejouand Y H 2013 *Elastic Network Models: Theoretical and Empirical Foundations Biomolecular Simulations* ed Monticelli L and Salonen E (Springer-Verlag) pp 601–616
- [48] May V and Kühn O 2011 *Charge and Energy Transfer Dynamics in Molecular Systems* (Weinheim, Germany: WILEY-VCH Verlag GmbH & Co. KGaA)
- [49] Morgan S E, Cole D J, Chin A W, Austin R H and Jansen T L C 2016 *Scientific Reports* **6** 36703